Available online at www.sciencedirect.com

SciVerse ScienceDirect

Ceramics International 38 (2012) 1533–1548

CERAMICS INTERNATIONAL

www.elsevier.com/locate/ceramint

Systematic approach to treat chronic osteomyelitis through ceftriaxone–sulbactam impregnated porous β-tri calcium phosphate localized delivery system

Biswanath Kundu [a], Samit Kumar Nandi [b,*], Subhasis Roy [b], Nandadulal Dandapat [a], Chidambaram Soundrapandian [a], Someswar Datta [a], Prasenjit Mukherjee [b], Tapan Kumar Mandal [c], Sudip Dasgupta [a], Debabrata Basu [a]

[a] *Bioceramics and Coating Division, CSIR-Central Glass and Ceramic Research Institute, Kolkata, India*
[b] *Department of Veterinary Surgery and Radiology, West Bengal University of Animal and Fishery Sciences, Kolkata, India*
[c] *Department of Veterinary Pharmacology and Toxicology, West Bengal University of Animal and Fishery Sciences, Kolkata, India*

Received 9 April 2011; received in revised form 13 September 2011; accepted 19 September 2011
Available online 24 September 2011

Abstract

Present investigation deals with *in vitro* and *in vivo* experimentation to treat chronic osteomyelitis, using pure β-tri calcium phosphate porous scaffolds. A novel approach was given to treat such infections using the scaffolds and drug combinations consisting of ideal antibiotics. *In vitro* studies include variation of porosity with interconnectivity, pore-drug interfacial studies by SEM-EDAX and drug elution studies both in contact with PBS and SBF at ca. 37 °C. *In vivo* trials were based on experimental osteomyelitis in rabbit model in tibia by *Staphylococcus aureus*. Characterizations included histopathology, radiology and estimation of drug in both bone and serum for 42 days by HPLC and subsequent bone–biomaterial interface by SEM. Samples having 60–65% porosity with average pore size ca. 55 μm and higher interconnectivity (22–113 μm), high adsorption efficiency (ca. 79%) of drug showed prolonged, sustained release of the drugs considered being sufficient to treat chronic osteomyelitis with desirable bone formation.

Keywords: Pure β-TCP; Ceftriaxone–sulbactam; *In vitro* and *in vivo*; Simulated body fluid; New Zealand white rabbits; Pore size

1. Introduction

Eradication of infection in chronic osteomyelitis constitutes infection control, soft tissue coverage, and bony union. Infection control is based on surgical debridement and prolonged antibiotic administration (4–6 weeks) [1]. In spite of the availability of a multitude of antibiotics and marked progress in surgical treatment, the long-term recurrence rate with osteomyelitis remains alarming at a rate of 20–30% [2]. The primary reason being the inability of conventional systems of drug delivery including injectables to achieve effective local concentrations; as infected bones are moderately perfused organs and experience uncertain blood circulation. Subeffective concentrations of antibiotics are the main cause for development of microbial drug resistance also. Due to the limited choices of available drugs [3] and difficulties of administrating them in infected site by conventional methods, the treatment of osteomyelitis is often a lengthy process with frequent serious side effects [4].

Local delivery of antibiotics with bone bioactive ceramics has proved to improve the prognosis of orthopaedic infections [5,6]. β-Tricalcium phosphate (β-TCP) is an impressive bioactive ceramic that could be applied as a carrier material in the design of bone drug delivery systems. It is biocompatible, bioactive, osteoconductive, osteoinductive [7], slow degrading, completely resorbable in variable period and with proven clinical effectiveness [8–10]. *In vivo* bone tissue ingrowth is affected by pore size, as it manipulates migration and proliferation of osteoblasts and mesenchymal cells and matrix deposition in the empty space [11]. Increasing porosity

* Corresponding author at: 37 and 68, Kshudiram Bose Sarani, Kolkata 700037, India. Tel.: +91 9433111065; fax: +91 33 25571986.
E-mail address: samitnandi1967@gmail.com (S.K. Nandi).

0272-8842/$36.00
doi:10.1016/j.ceramint.2011.09.038

of β-TCP from 20 to 40% has been reported to extended drug release from one and half days to three weeks [12]. However, osteomyelitis demands drug for a period of 4–6 weeks [1].

Various classes of antibiotics as cephalosporins, fluoroquinolones, β-lactams, glycopeptides etc., have been studied for their effectiveness against osteomyelitis. It has been reported that cephalosporins is not appreciably effective in osteomyelitis due to the β-lactamase production of the main causative agent, *Staphylococcus aureus*. However, drug combinations that include an irreversible β-lactamase inhibitor with β-lactam antibiotics, proves to be a rational counter approach in the treatment of infections caused by β-lactamase producing strains [13,14]. Ceftriaxone (CFT) is a cephalosporin that has lost its clinical popularity. But has recently been reported to exhibit better bactericidal activity, *in vitro* and reduced probability of resistance development, in combination with sulbactam (SUL), a β-lactamase inhibitor [15]. For the treatment of chronic osteomyelitis because of their favourable intrusion into poorly vascularized sites of infection, their advantageous bactericidal effects against all probable pathogens of chronic osteomyelitis with lack of serious adverse reactions, this drug combination of CFT and SUL was selected [16].

To address the above concerns, this investigation was designed for a systematic and extensive study focused on: (1) development of highly interconnected porous β-TCP scaffold with two variations of porosity, (2) development and detailed characterization of combined drug ceftriaxone–sulbactam (CFS) impregnated β-TCP porous scaffold, (3) *in vitro* drug release efficiency in both PBS and SBF and finally, (4) *in vivo* animal trial to check the efficacy of selected type of porous β-TCP scaffold loaded with novel drug combination (CFS) to combat chronic osteomyelitis and aid new bone formation.

2. Materials and methods

2.1. Fabrication and characterization of pure β-TCP based porous scaffolds

Pure β-TCP powder was synthesized at 80 °C in the laboratory by a wet chemical method using analytical reagent grade calcium carbonate and ortho-phosphoric acid as the initial reactants with the Ca/P molar ratio of ca. 1.5. Details of this synthesis could be found elsewhere [17]. Powders calcined at 800 °C were used for fabrication of porous scaffolds. Porous samples were fabricated by modification of a process, developed by us earlier [18] using scintillation grade naphthalene (SD Fine-Chem, India) as pore former. In the present investigation, naphthalene was added at two different percentages of the scaffold formulation, viz., 50 and 60%, (hereinafter the same designated as 50P and 60P). The powder mix was subsequently compacted at a pressure of 150 MPa (for 40 s) by cold-isostatic pressing (EPSI N.V.; SO 10036, Belgium) to form cylindrical shaped green specimens. By very slow heating up to 80 °C, the naphthalene was driven off from the green specimens with care to prevent cracking, at this stage. Finally, the green and fragile specimens were sintered at 1200 °C for 1 h. Physical properties including apparent or open porosity as well as bulk density of the sintered porous specimens were measured by Archimedes' principle. X ray diffraction (XRD) (Philips Analytical B.V., X'Pert Pro, Netherlands) was performed for analyses of phase/s while Fourier transformed infra-red spectroscopy (FTIR) (Perkin-Elmer, Spectrum 100, USA) were taken for confirmation of required functional groups. Surface charge in terms of zeta potential of the sintered powder aqueous suspensions was also estimated for indirect estimation of interaction between these particles and CFS by the standard method [19]. Microstructure of porous scaffolds was observed by field emission scanning electron microscopy (FESEM) (Carl Zeiss, Supra 35 VP, Germany) on one side of the flat-parallel surface. Image analysis was carried out to calculate the pore size distribution (Perfect Screen Ruler 2.0, Styopkin Software, USA). More than 250 linear measurements were taken from each micrograph and converted to their actual dimension from the corresponding tag of each microstructure. Histograms thus obtained were plotted as function of pore size ranges. The average pore sizes were also determined.

2.2. Fabrication and characterization of drug impregnated scaffolds

We have used a combination of two drugs CFT and SUL in 2:1 ratio, because this is recommended dosage usually prescribed for the parenteral treatment of chronic bone infections. Five numbers of samples for each kind of porous scaffolds were soaked in a solution of CFS (500 mg/mL concentration) prepared in ultra-pure water (Milli-Q Academic Century, ZMQS50001, China) and subjected to a vacuum of 10 mm Hg for at least 30 min. The samples were further freeze dried (Eyela, FDU-2200, Japan) and checked for adsorption efficiency. This was expressed as percentage (the change in weight of TCP scaffold before and after drug impregnation work divided by the weight before impregnation) [20]. A section of these CFS impregnated porous blocks were characterized for microstructural evolution using an SEM. Depending on the samples' composition, microstructures were taken either in secondary electron or back-scatter electron mode. For assessment of the compositional variation along the interface between pore surface and drug, energy-dispersive analysis of X rays (EDAX) (vacuum: 1.14×10^{-6} mbar, beam current of electron gun: 1.0 nA, spot size: 520 nm, working distance: 8.5–9 mm, SiLi detector and collection time: 45 s) were taken. Depending on the microstructure observed, line-scan of EDAX was performed for compositional variation and compared with the said microstructure.

2.3. In vitro drug release studies

In vitro drug elution studies were performed in two liquid media PBS and SBF. PBS used was a solution of salts as NaCl (137 mM), KCl (2.7 mM), Na_2HPO_4 (10 mM), KH_2PO_4 (1.8 mM) with a pH of 7.4 while SBF was prepared in accordance to Kokubo et al. with ionic concentrations equal to

human blood plasma [21]. CFS impregnated scaffolds were placed in test tubes containing 3 mL of liquid medium and stored in a thermostatic chamber at ca. 37.4 °C. After each day up to 7 days and each week subsequently up to 42 days, the samples were removed and transferred to a new tube containing 3 mL of fresh liquid medium. The liquid media containing the released CFS were stored at −80 °C until analysed. After filtration, the amount of CFS release was determined by HPLC (Shimadzu, SPD-MIOA, Japan) fitted with binary pump (LC-20 AT), diode array detector. Similar procedures were followed for obtaining the assays up to 42 days. The conditions for HPLC were as follows: for determination of CFT, the mobile phase was composed of HPLC grade water:acetic acid:acetonitrile ca. 70:5:25 with flow rate 1 mL/min and detection wavelength 254 nm. The separation was carried out using an RPC_{18} pH stable column (Phase Separations, Norwalk, CT), 15 cm long. For determination of SUL, the mobile phase was a mixture of buffer:acetonitrile ca. 88:12 (the buffer was a solution of 0.1 M KH_2PO_4, tetra-butyl-ammonium hydroxide and 0.1 M phosphoric acid). The flow rate was 1.5 mL/min with detection wavelength of 313 nm. Percent yield [20] of CFS was expressed as the total amount of released antibiotic divided by the amount of CFS held in the samples before the start of elution in PBS and SBF separately.

2.4. In vivo studies

S. aureus (coagulase positive) obtained from an animal infected with chronic osteomyelitis was used for development of experimental model in rabbit. Pure cultures of the bacteria were obtained on blood agar at 37 °C and standardized suspensions (3×10^6 CFU/mL) prepared in saline. This sample (1 mL) was introduced into the medullary cavity of rabbit tibiae for successful induction of osteomyelitis by *S. aureus* and the same confirmed by manitol salt agar test. Animal experimentations were carried out following the procedures conforming to the Standards of the Institutions Animal Ethical Committee of the West Bengal University of Animal and Fishery Sciences, India. Osteomyelitis was induced in the right tibia of 24 (twenty four) nos. of New Zealand white rabbits (2.5–3 kg body weight) according to the model of Norden [22]. The proximal part of the tibia was exposed anteriorly after anaesthesia with Nembutal 0.5 mg/kg intra-venous (IV) (Thiopentone sodium, Thiosol®, Neonlab, Mumbai, India), and a hole was drilled through the cortex into the medullary cavity using a 1.2 mm diameter dental burr. 1 mL of *S. aureus* suspension containing approximately 3×10^6 CFU/mL was injected into the drilled medullary cavity and the hole was sealed with bone wax to prevent bacterial leakage into the surrounding soft tissues. The animals were monitored after surgery. All the animals received standard postoperative pain medication (Carprofen; 4 mg/kg of body weight) for 3 days. The animals those developed osteomyelitis after three weeks of inoculation were only considered for present study. CFS impregnated β-TCP scaffolds (samples from 50P series) were implanted in the infected bone and same postoperative management were followed. The twenty-four animals were divided into 3 groups hereinafter would be designated as groups I–III. The details of the experimentation model with these animals are tabulated (Table 1). All the samples required for the study parameters were obtained on 12, 21 and 42 days post osteomyelitis. Thoroughly washed 3–4 mm thick sections of implanted bone/antibiotic impregnated β-TCP implants were fixed in 10% formalin for 7 days and subsequently decalcified in Goodling and Stewart's fluid containing formic acid 15 mL, formalin 5 mL and distilled water 80 mL solution. Haematoxylin and eosin stained decalcified cross sections were considered for histological examinations. Radiographic images of the subjected bones were taken under direct radiographic magnification. Blood samples from the ear vein and pulverized, homogenized, centrifuged supernatant fluid from cortico-cancellous portion of tibia (removing bone marrow) were collected for estimation of antibiotic (CFS) by HPLC techniques by the methods described earlier. The results were expressed as means ± standard deviations. Specimens were also collected for SEM analysis from the cortical part of the bone of animals from all the three groups after 42 days; while from Group II samples were also collected after 21 days,

Table 1
Design of experiment for *in vivo* animal experimentation.

Group	No. of animals	Implant	Days of experiment	Experiment
Group I	6	Not given	21	Six animals were sacrificed for histological, radiographic and microbiological examination to confirm development of osteomyelitis.
Group II	9	CFS injection parenterally (15 mg/kg, bid) twice daily for 6 weeks	12	Three animals were sacrificed for histological and estimation of drug concentration in bone and serum.
			21	Three animals were sacrificed for histological and estimation of drug concentration in bone and serum.
			42	Three animals were sacrificed for histological, radiographic, and estimation of drug concentration in bone and serum.
Group III	9	CFS loaded β-TCP porous scaffolds	12	Three animals were sacrificed for histological and estimation of drug concentration in bone and serum.
			21	Three animals were sacrificed for histological and estimation of drug concentration in bone and serum.
			42	Three animals were sacrificed for histological and estimation of drug concentration in bone and serum.

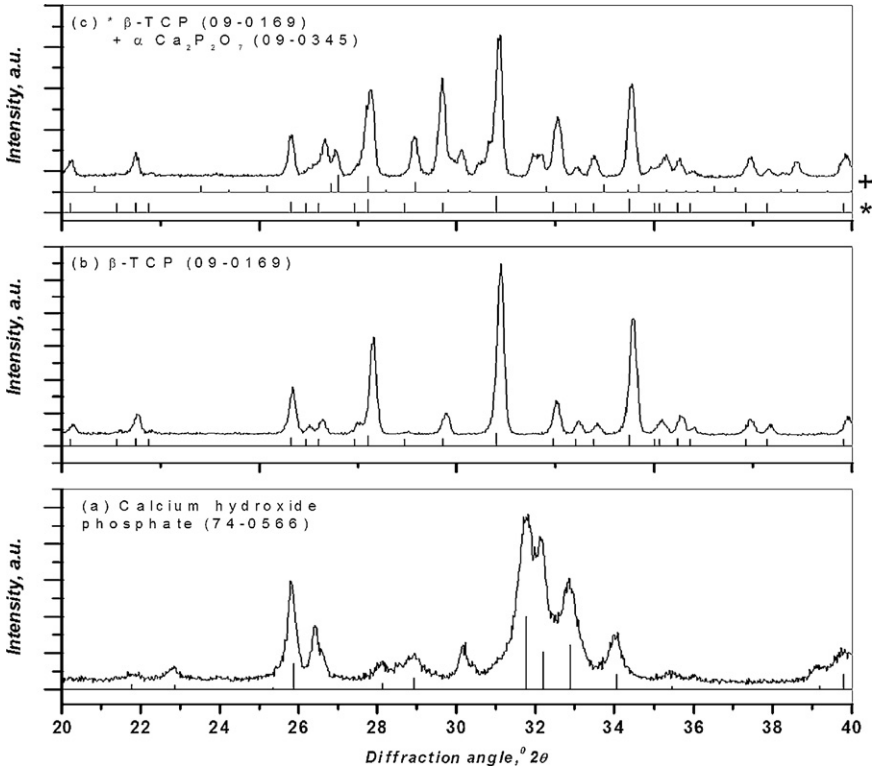

Fig. 1. XRD of (a) as-prepared (at 80 °C), (b) 800 °C calcined and (c) 1200 °C sintered powder.

post-operatively. For SEM specimens, 5% glutaraldehyde phosphate solution was used for fixing the samples, washed twice for 30 min with PBS (pH 7.4) and distilled water, dehydrated in a series of graded ethanol followed by final drying with hexamethyldisilizane (HMDS). A gold conductive coating was given by ion sputtering (JEOL ion sputter, Model JFC 1100, Japan) at 7–10 mA and 1–2 kV for 5 min. The resin mounted sample surfaces were then examined under SEM (JEOL JSM 5200 model, Japan) after proper alignment.

3. Results and discussion

Details of the phase analysis could be found elsewhere [17], but, very briefly, from XRD (Fig. 1) analysis it was found that the as-dried powder (80 °C) was converted to pure β-TCP [matched with standard in JCPDS PDF (Joint Committee on Powder Diffraction Standards Powder Diffraction Files) no. 09-0169] when calcined at 800 °C and finally a secondary phase (matched with PDF no. 09-0345) appeared when fired at even higher temperature, viz. 1200 °C (the sintering temperature for TCP). This was α-calcium pyrophosphate (α-$Ca_2P_2O_7$). Percent of phase content for this composite phase was calculated by using internal standard method [23] with mass absorption coefficient values of β-TCP, α-$Ca_2P_2O_7$ and composition consisting of β-TCP and α-$Ca_2P_2O_7$ were taken as 95.59, 76.99 and 81.83 respectively. Sintered β-TCP was composed of ca. 59.5 and 14% of β-TCP and α-$Ca_2P_2O_7$ respectively, while 800 °C calcined powders were ca. 83.5% β-TCP. Rest was the amorphous calcium phosphate. This amorphicity again was calculated by taking the ratio of XRD peak for coherent scattering to background (i.e. incoherent scattering) w.r.t. the standard material for β-TCP [24]. Amorphous content in the fabricated materials were increased from ca. 16.5–26.5% when it was fired to its sintering temperature (i.e. from 800 to 1200 °C). These parameters were important for the study of drug impregnation subsequently. FTIR spectrum (Fig. 2) of the powders calcined at different temperatures on the other hand in the range of 800–1200 cm^{-1} showed wide transmission band typical of tetrahedral anions XO_4^n, in particular, PO_4^{3-}. FTIR analysis demonstrated PO_4^{3-} transmission peaks around 945, 1040–1122, 601 and 552 cm^{-1} attributable to β-TCP [25]. No structural OH^- could be noticed. Phosphate ions had four vibration modes viz. ν_1, ν_2 (961), ν_3 (1119 and 1044) and ν_4 (601) [26,27]. Band positions like 2926 and 2854 cm^{-1} resembled presence of OH functional group [28], which was not incorporated into the crystal structure.

Physical parameters of the porous TCP scaffolds are given in Table 2. It was found that the increase in naphthalene content in the formulation resulted lower porosity and hence higher bulk density in 60P samples. Further, increase of naphthalene by 10% resulted in decrease of open porosity by 8%. SEM microstructures of the 50P and 60P samples are presented in Figs. 3 and 4. Histograms based on image analysis are presented in Fig. 5. The microstructures were very non-uniform with high interconnectivity of pores. 60P samples had granular microstructures with large amount of micropores. A bimodal distribution of pores was seen for 50P samples. Both micro- (<50 μm) and macro-pores (>50 μm) were evidenced from both the micrographs with higher amount of macro-pores in 50P samples than 60P. The average pore sizes were found to be

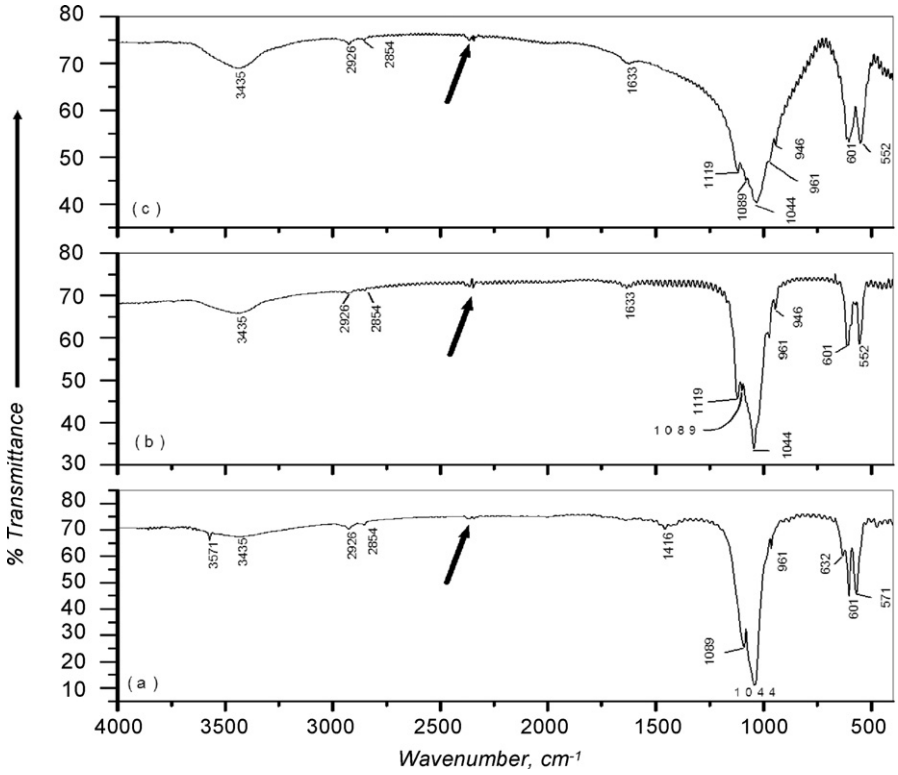

Fig. 2. FTIR of (a) as-prepared (at 80 °C), (b) 800 °C calcined and (c) 1200 °C sintered powder.

ca. 55.1 and 57.3 μm for 50P and 60P samples respectively. It was noticed that with increasing amount of naphthalene, the spherical nature of pore shapes (when the naphthalene percentage was only ca. 5–10%) started to change and the void shapes were ruptured (when the naphthalene percentage was ca. 30%). More and more non-uniform release of this fugitive material was evident and so the microstructures. This secondary phase and amorphous content in the sintered body played a role (forming an eutectic liquid at that temperature) for reduction of porosity, interconnectivity and subsequent pore structure collapse with further addition of ca. 10% naphthalene from 50P to 60P samples [29]. Interconnected pores were found in all photomicrographs. Sub-surface interconnections were found in the range from 15 to 94 μm throughout the microstructures of 60P samples and about 22–113 μm for 50P samples.

Adsorption efficiency of the drug CFS for 50P and 60P samples were on an average found to be ca. 79 and 66% respectively. Efficiency increased with increase of pore percentage and distribution of pores. Due to increase of the surface area of the pores, the drug adsorption efficiency was increased for 50P samples. With increase of crystallinity, the degree of attachment of drug decreases. With the decrease of crystallinity of calcined (800 °C) TCP powders to 77% at the selected sintering temperature, the degree of attachment of drugs may be expected to be high with the porous scaffold when sintered. Surface charge in terms of zeta potential for β-TCP (fired at 1200 °C) with varying pH had a high negative potential throughout the observed pH spectrum and hence, in the physiologic pH spectrum it will behave as anionic. Surface charge had a definite role for adsorption to the surface of porous TCP as well as the cohesion between drug CFS and calcium phosphate. We have also studied the surface morphology of TCP scaffolds loaded with drug (Fig. 6-I). The SEM photomicrographs showed microstructure of crystalline TCP

Table 2
Physical parameters of the porous scaffolds before drug impregnation.

Sample	Bulk density, g/cm^3	Apparent porosity, %
50P	1.16 ± 0.07	61.39 ± 3.51
60P	1.39 ± 0.05	53.26 ± 1.27

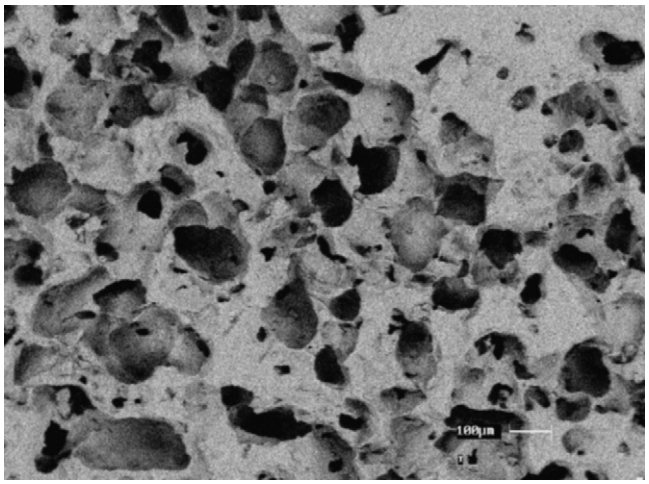

Fig. 3. SEM microstructure of 50P samples.

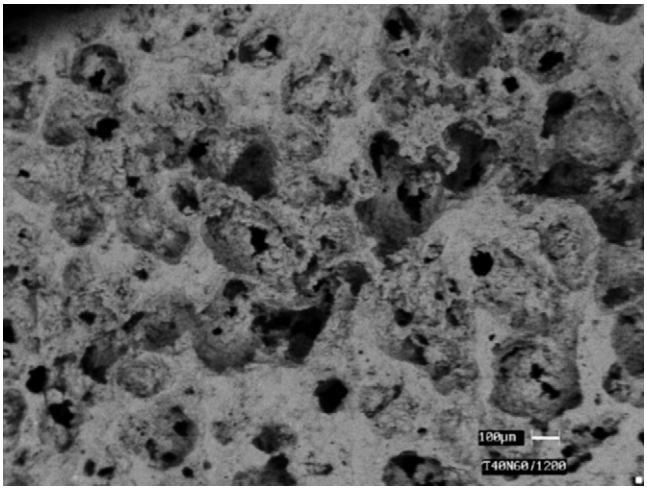

Fig. 4. SEM microstructure of 60P samples.

and indistinguishable closest approximated drug at the interface infused into the pores. Cracks were visible at the drug surface only (marked with white arrow). Corresponding EDAX taken at regions of differing contrast are given in Fig. 6-II a and b and crosschecked for compositional variation (if any). In the black area of microstructure of Fig. 6-I, there were elements like S (sulphur), Na (sodium), nitrogen (N) and carbon (C) with complete absence of peak corresponding to Ca, P and O (Fig. 6-II a). This indicated the prevalence of drug molecules (CFS) in those areas. White part of the microstructure of Fig. 6-I had abundance of Ca (calcium), P (phosphorous) and O (oxygen) as obtained in Fig. 6-II b, which correspond the TCP structure. There were no interfacial cracks/gap between the TCP and infused drug. Release profiles of the drugs CFT and SUL in PBS and SBF are plotted separately in Figs. 7 and 8 respectively. On an average, it was found that the drug yield after 42 days of elution in contact with PBS were ca. 73.6% and 59.2% for 50P and 60P samples respectively. There was a high release of drugs observed initially from all the samples followed by a much restricted release profile. There was ca. 0.83 and 0.54 mg/mL of CFT and 0.14 and 0.1 mg/mL of SUL release in the very first day for two kinds of samples, the rate was subsequently

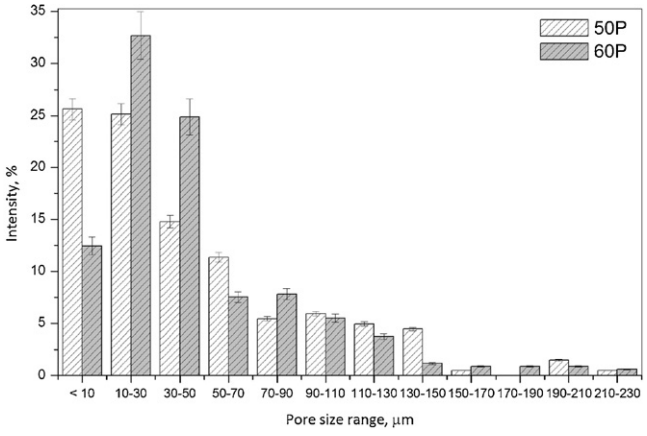

Fig. 5. Histogram showing the pore size distribution of 50P and 60P samples.

dropped down up to 4th day and subsequently the release become very slow and continued up to 42 days. Faster and more uniform drug release profile was observed for 50P samples owing to its higher percent porosity, interconnected pore sizes and bimodal distribution of pores. On the other hand, in contact with SBF, higher releases of both the drugs were observed in the total study period (Fig. 8) of 42 days. Percent drug yield on an average was found to be ca. 98 and 80.9% for 50P and 60P samples respectively. There was higher burst release of the individual drugs in the first day (2.54 and 3.58 mg/mL CFT and 0.98 and 2.81 mg/mL SUL from 50P and 60P samples respectively) in contact with SBF, but the rate of release was very uniform until 42 days. After 42 days, higher CFT release was observed for 50P samples than 60P samples. PBS had less effect on the drug elution rate for all the samples than SBF. In general, the elution rate of the drug CFS was much faster throughout the study period for SBF than PBS.

In vivo, histological section on third week in Group I revealed bony degeneration of haversian plates. Medullary sinuses showed infiltration of mononuclear cells and few osteoblasts. The margin of sinuses is getting eroded in some places [5]. Osteoclastic activity in some interstitial spaces is also evident and all the phenomena were the indicative of osteomyelitis (Fig. 9). Sections taken on 12 days from Group II showed fibropurullent reaction with mucin deposit and presence of polymorphonuclear cells. Some portion of medulla was replaced by cellular clumps of mononuclear cells with eosinophilic exudation. The vascularity of the cortico-medullary junction was scanty indicating a persistent infection. The presence of giant cells indicated the chronicity of the disease (Fig. 10a). The histologic section on 21 days showed a degenerative stage of bony lamina with scanty cellular reaction. In between laminae, there was also evidence of exudation with edematous fluid, but, the other structures were indistinct (Fig. 10b). On day 42, formation of partial callus around the osteoid was noticed. The Haversian system retained their structures. Vascularity of the bony parenchyma was moderate (Fig. 10c). These histological findings suggest that there was only a minimal reaction towards biomaterial and gradual new bone formation in the area. Histology on day 12 in Group III showed bundles of fibrous tissue encircling the bony laminae along with normal osteogenesis and cartilagenesis (Fig. 11a). Other bony structures were retained normal. Whereas, on day 21 the section showed clearly marked bony laminae and haversian system. The medulla showed mild osteogenesis in the pericortical surface. Osteocytes were seen in proliferating stage (Fig. 11b). The section on day 42 in same group illustrated bony parenchymal structures in remodelling phase of osteoids, comprising of cartilagenous cellular proliferation along with fibrovascular structures. Few bony macrophages showed engulfment of tissue debris of bony parenchyma, but, vascular proliferation was moderate (Fig. 11c). The reason could be that CFS was released at an adequate concentration in the osteomyelitis site and controlled the infection which subsequently helped in new bone formation. Radiologically, osteomyelitis was inducted successfully in animals of all groups by inoculating *S. aureus* as evidenced by radiograph

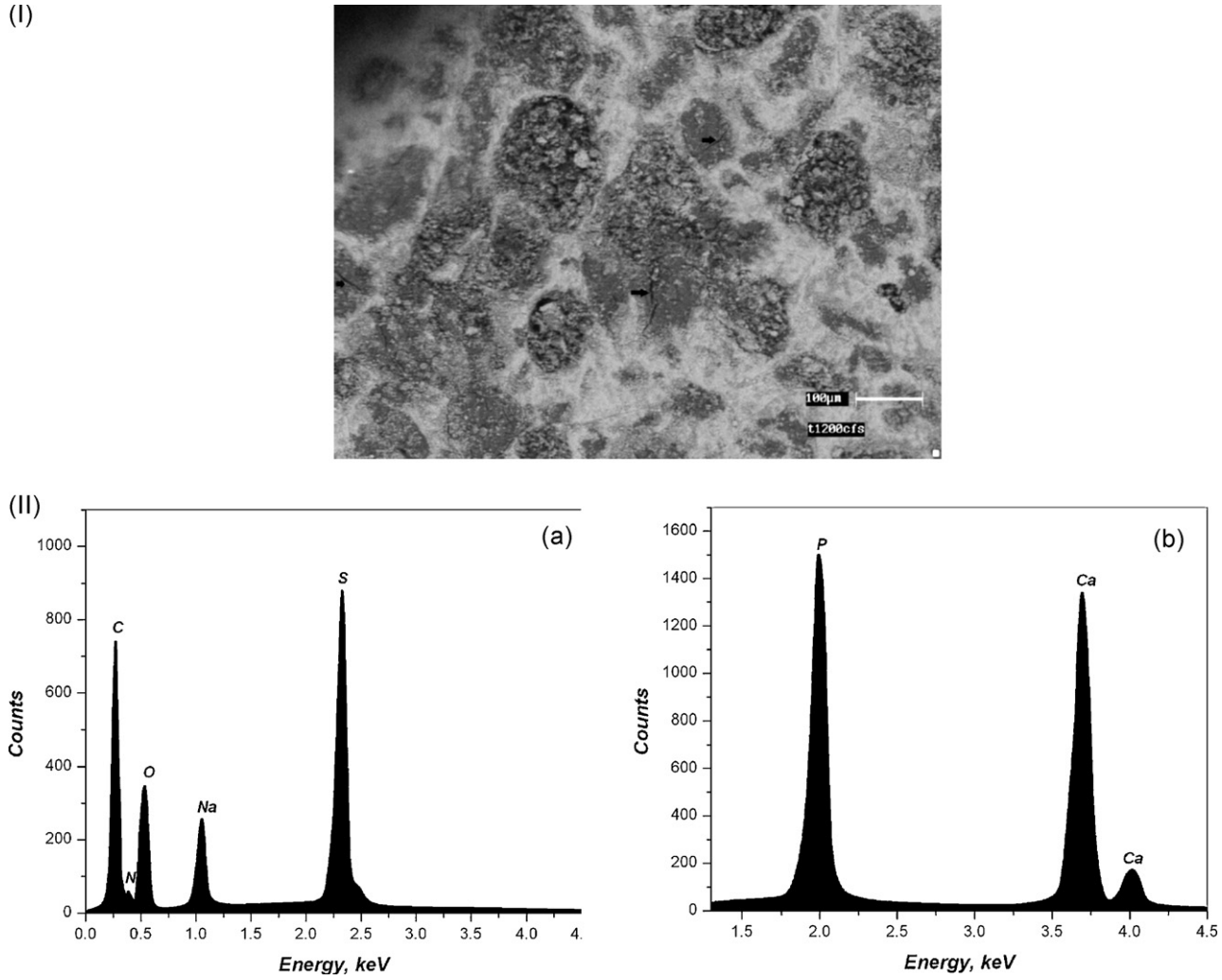

Fig. 6. I. SEM morphology of CFS drug loaded 50P samples. Black arrow is the crack on the CFS surface. II. EDAX taken on the surfaces shown in I. (a) Black region and (b) white region of I.

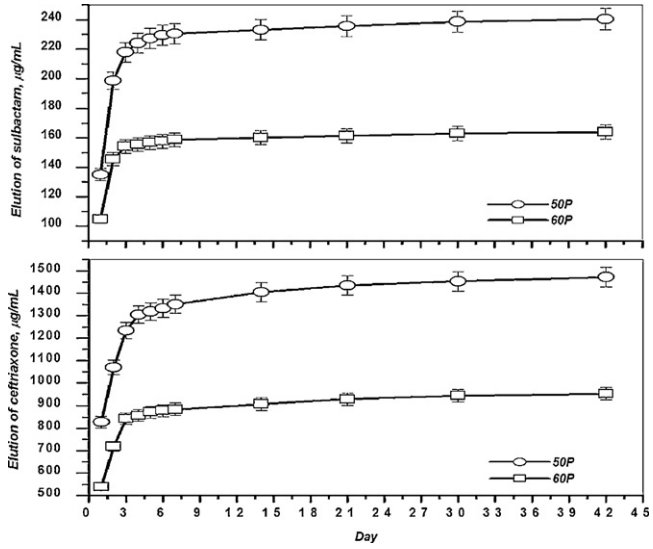

Fig. 7. Drug elution profile for 50P and 60P samples obtained up to 42 days in contact with PBS buffer (pH 7.4 and 37 °C). CFT and SUL are shown separately.

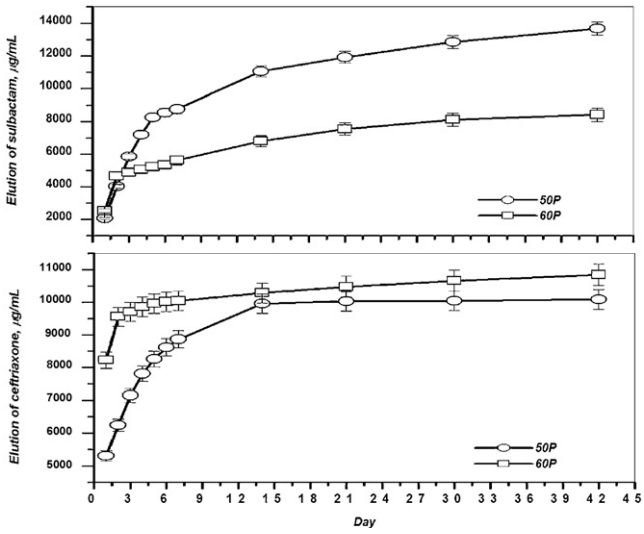

Fig. 8. Drug elution profile for 50P and 60P samples obtained up to 42 days in contact with SBF (pH 7.4 and 37 °C). CFT and SUL are shown separately.

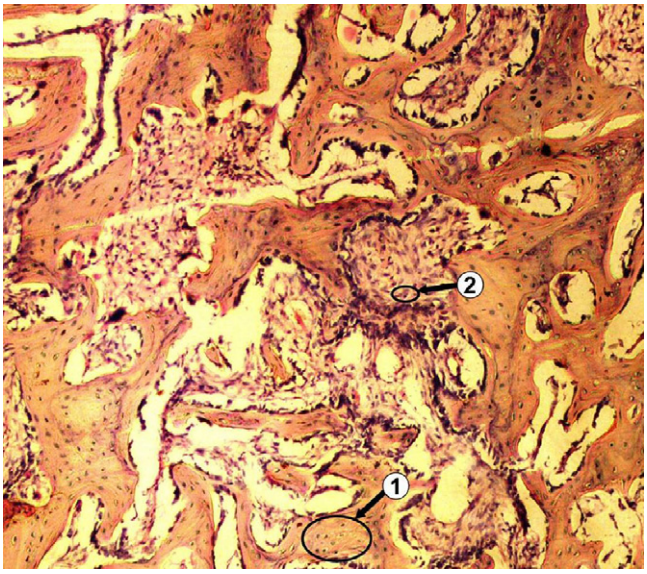

Fig. 9. Histological section of the Group I animal after 21 days (HE × 10); 1. haversian plate, 2. osteoclast.

(Fig. 12). There was severe periosteal reaction in the posterior aspect of proximal metaphysis with the evidence of radiodense lamellated new bone formation from periosteum. In some places lytic changes and thinning, even disappearance of cortex leading to formation of radiolucent zones were evident, whereas, in some places of proximal metaphysis of tibia characteristic appearance of spongy bone was not evident. Radiodensity of bone marrow appeared to be more with prominent endosteal reaction. In Group II animals, the radiograph on 12 days showed increased radio-opacity along with loss of characteristics of cancellous bone in proximal metaphysis of tibia. Both the phytic and lytic changes were prominent in proximal metaphysis. Formation of new bone was of amorphous type. Moderate endosteal reaction was clearly visible. Anterior cortical border of proximal metaphysis of tibia showed discontinuation in some places. Epiphyseal cartilage showed secondary osteophytic changes (Fig. 13a). The radiograph on 21 days showed variable radiodensity in anterior border of proximal metaphysis along with discontinuation of cortex in few places. Endosteal reaction was mild. Reestablishment of the medullary cavity and remodelling of cortex were noticeable (Fig. 13b). On 42 days the radiograph showed few radiolucent zones characteristic of osteoclastic changes.

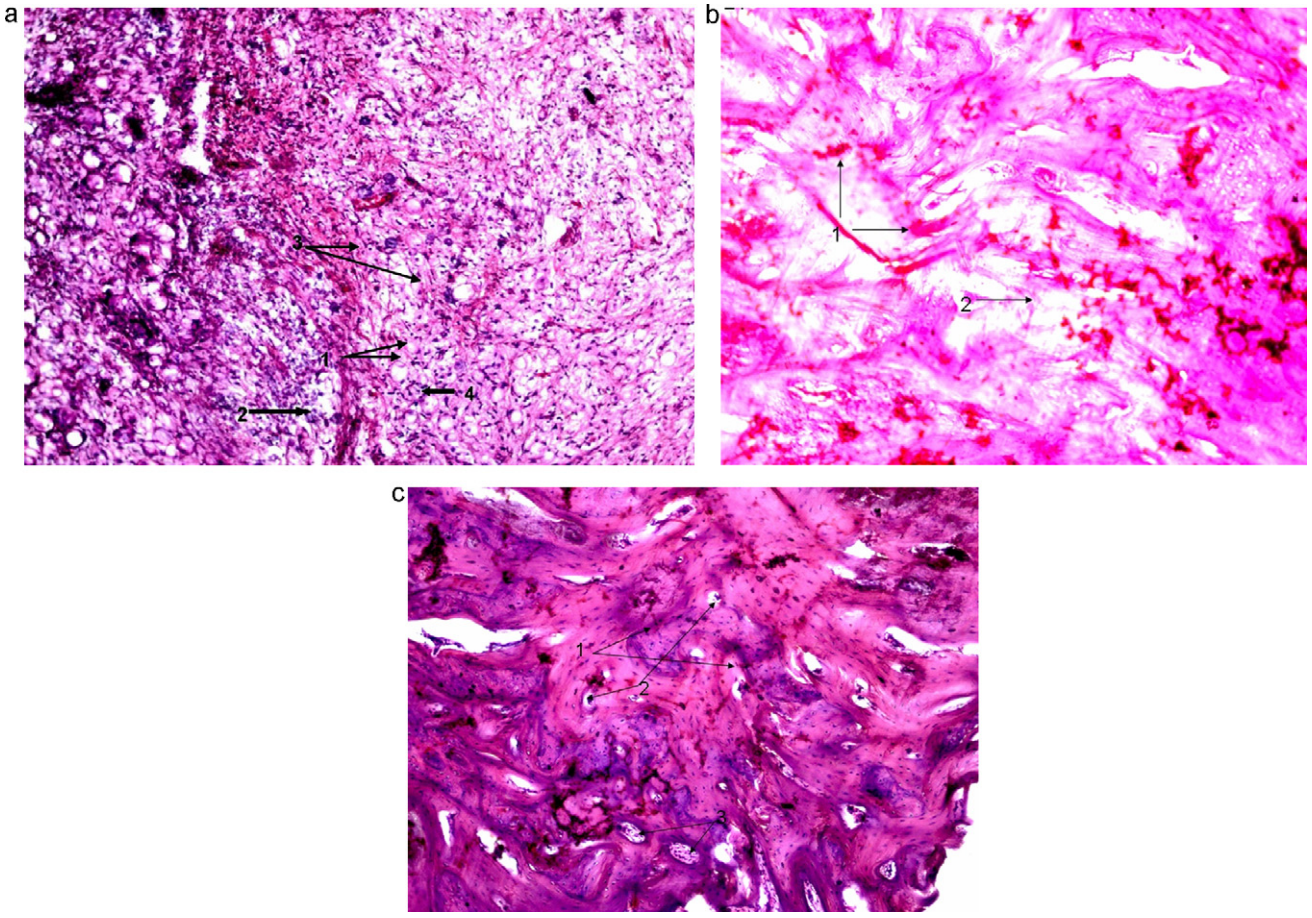

Fig. 10. (a) Histology of the Group II animal after 12 days (HE × 10). The section shows fibropurullent reaction with mucin deposit (1) and presence of polymorphonuclear cells (2). Some portion of medulla is replaced by cellular clumps of mononuclear cells with eosinophilic exudation (3). Presence of giant cells (4) indicate the chronicity of the disease. b. Histology of the Group II animal after 21 days (HE × 10). (1) Degenerative stage of bony lamina; (2) Exudation with edematous fluid. c. Histology of the Group II animal after 42 days (HE × 10). (1) Formation of partial callus around the osteoid; (2) Haversian system retains their structure; (3) Vascularity of the bony parenchyma is moderate.

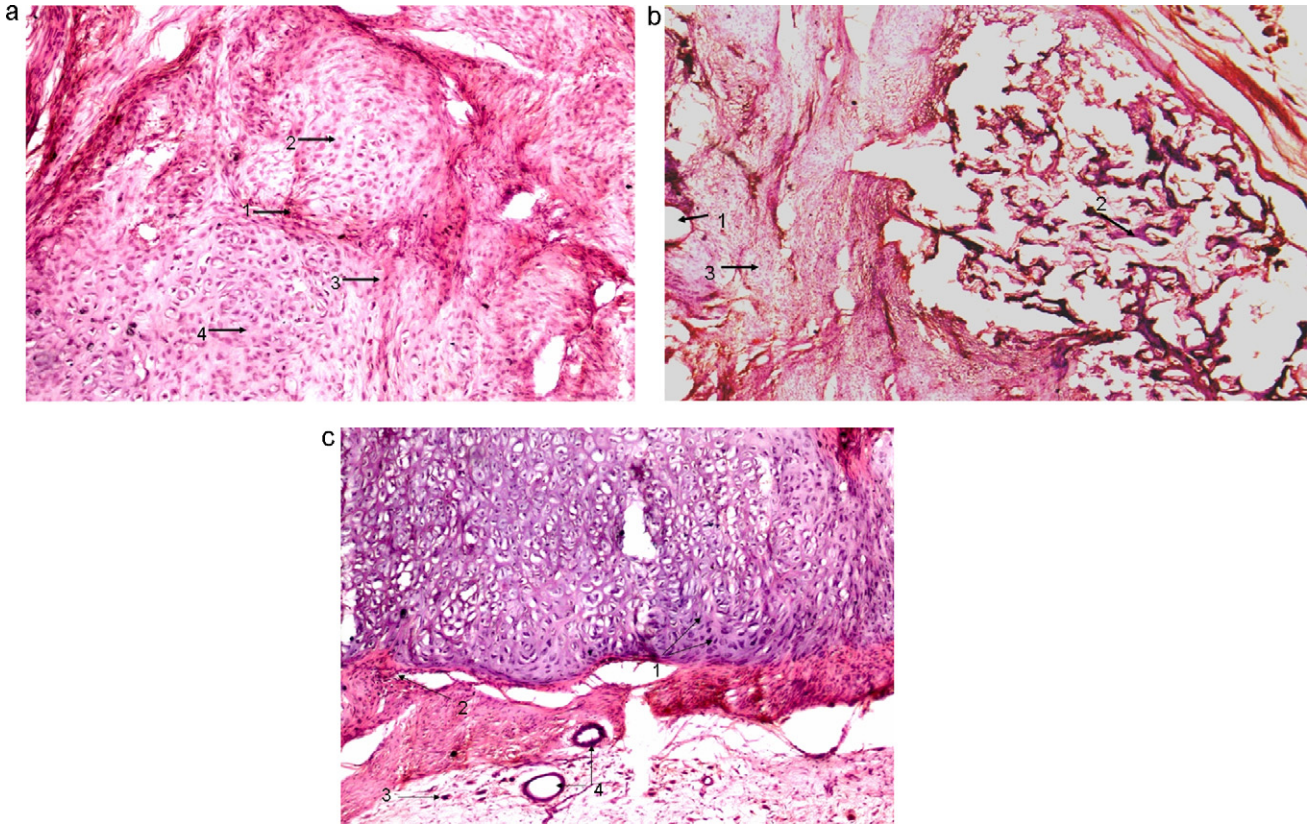

Fig. 11. (a) Histology of the Group III animal after 12 days (HE × 10). (1) Bundles of fibrous tissue; (2) bony laminae; (3) osteoblast and (4) cartilagenesis. b. Histology of the Group III animal after 21 days (HE × 10). (1) Bony laminae and haversian system; (2) mild osteogenesis in the pericortical surface; (3) osteocytes. c. Histology of the Group III animal after 42 days (HE × 10). (1) Cartilagenous cellular proliferation; (2) fibrovascular structure; (3) few bony macrophages; (4) vascular proliferation is moderate.

Absence of periosteal and endosteal reaction, reestablishment of medullary cavity along with cortical continuation demonstrated the radiograph as under process of healing (Fig. 13c). Finally, Group III radiograph on day 12 showed circular, intact antibiotic impregnated TCP block at proximal diaphysio-metaphyseal junction with variable radiodensity. Radiographically the appearance of spongy bone in proximal metaphysis of tibia was not uniform. In some places of proximal metaphysis, lytic changes were visible. Radiodensity of medullary cavity throughout the tibia was dissimilar. In few places some osteophytic changes along with mild periosteal reaction was demonstrated, but, no endosteal reaction was seen (Fig. 14a). The lateral radiograph on day 21 unabsorbed, round radio opaque TCP implant with continuation of periosteum was visible. In some places of proximal metaphysis, lytic changes were prominent. Radiographically, periosteal reaction was absent. Reestablishment of medullary cavity was near to complete (Fig. 14b). Encircling radiolucent zone around the implant-host bone was not visible compared to the previous radiograph. Whereas, the radiograph on 42 days showed mostly absorbed moderately radio-opaque TCP implant. Complete reestablishment of medullary cavity was clearly visible. No osteophytic changes were radiographically demonstrated. Metaphyseal spongy bone was visible in proximal metaphysis. The radiograph was devoid of any osteomyelitic changes (Fig. 14c).

Fig. 15a shows that serum concentrations of CFT were 14.01, 15.9 and 12.84 μg/mL on day 12, 21 and 42 following twice daily parenteral administration at 15 mg/kg in rabbits. But, the concentration of CFT in bone on respective days was significantly lower suggesting lesser distribution of CFT from blood/serum to bone. However, an MIC of 2.0 μg/mL was maintained in both serum and bone till day 42 of observation period after a total dose of more than 3000 mg in a rabbit (group II). On the other hand, higher concentration of 45.23 μg/g was recorded at day 12 followed by decline in concentration on days 21 and 42 (above 30 μg/g) after impregnated TCP bead in bone (group III), while serum concentration started to increase from 16.75 μg/mL at day 12 and maximum concentration in serum was found to be 49.65 μg/mL on day 42 indicating release of CFT from bone to blood/serum and the concentration in both bone and serum was significantly higher compared to animals of group II. Fig. 15b depicts the concentration of SUL in serum and bone on different days following parenteral and impregnated TCP beads implanted. Likewise CFT, SUL has also very less penetration capacity from blood/serum following twice-daily administration for 42 days observation period. On the other hand, concentration of SUL in bone was higher on day 12 which was decreased rapidly on day 21 and again increased on day 42 after implantation in bone. The serum concentration of sulbactam was inversely related with concentration in bone on different days suggesting excellent diffusion capacity of

Fig. 12. Radiograph of the Group I animal.

SUL into blood. From Fig. 15a and b, it may be concluded that a single β-TCP implanted CFT and SUL in bone causes sustained release of both drugs in bone and serum for 42 days observation period compared to conventional dosage form with very much higher amount of drug to maintain the MIC.

Microstructures of bone defect sites for all the group of animals are given in Fig. 16a–d. Fig. 16a and b displays the status of bone after 42 days when no treatment was provided (Group I) after development of osteomyelitis (i.e. control) and the site when parenterally treated (Group II) by CFS, respectively. Fig. 16c and d portrays the status of bone after 21 and 42 days when implanted with drug loaded porous TCP implants (Group III). It was observed that after 42 days in group I, there was abundance of RBC cells together with decalcification of the bony matrix, indicative of osteolytic activity of the *S. aureus* at the control site. There was insignificant presence of bridging callus and fibro cartilaginous tissues at the centre of the defect which indicates that mature bone cells formation was not completed after parenteral treatment of 42 days. On the other hand, drug incorporated porous 50P TCP sample showed reticulo formation and spreading of collagenous structure and penetration of bony trabeculae into the porous structure by 21 days and complete absence of any RBC cells indicating faster bone mineralization with no reincarnation of the bacteria at the defect site. By 42 days, matured bone covered the defect site where regularly arranged osteons at the edge of the pores were noticed. Inside of such implant also, there were no abstract collagenous tissues, indicating bone mineralization process was also completed inside. Vascularization by bony tissue was completed by 42 days.

Several antibiotics together with porous calcium phosphates scaffolds have been tried as delivery system to treat chronic osteomyelitis [12,30,31]. Hitherto, to the best of our knowledge, this is the first report of comprehensive and integrated study that evaluates the impact of pure β-TCP matrix having different pore conditions (which include pore percentage, size, morphology and most importantly interconnectivity and distribution of such pores), incorporating a rational antibiotic combination, with an extensive six week evaluation of *in vitro*

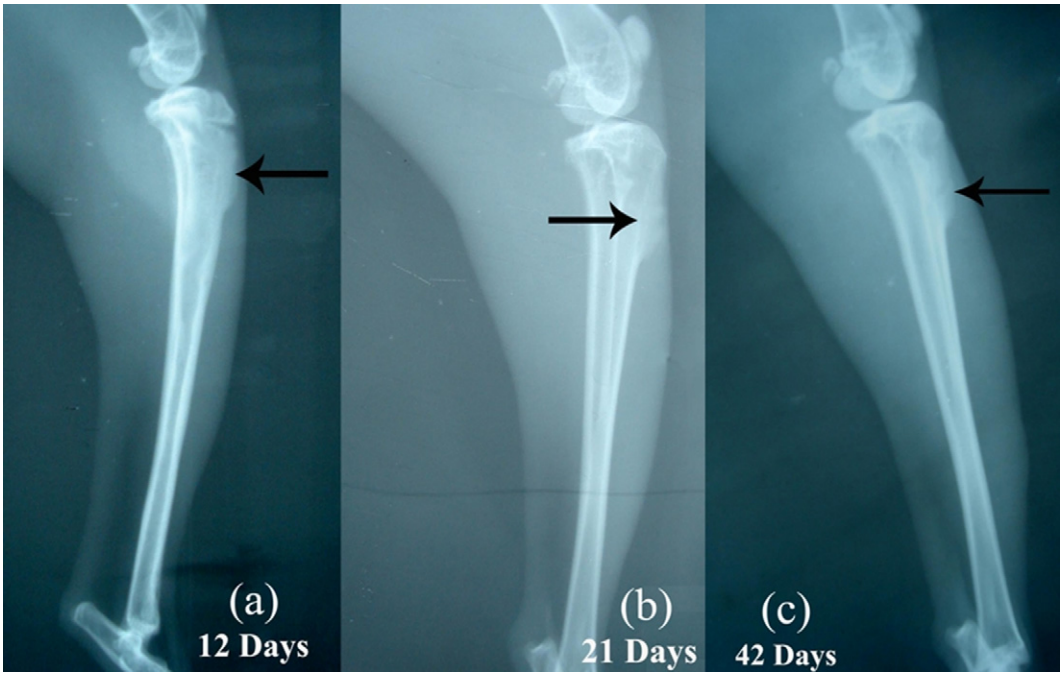

Fig. 13. Radiograph of the Group II animal.

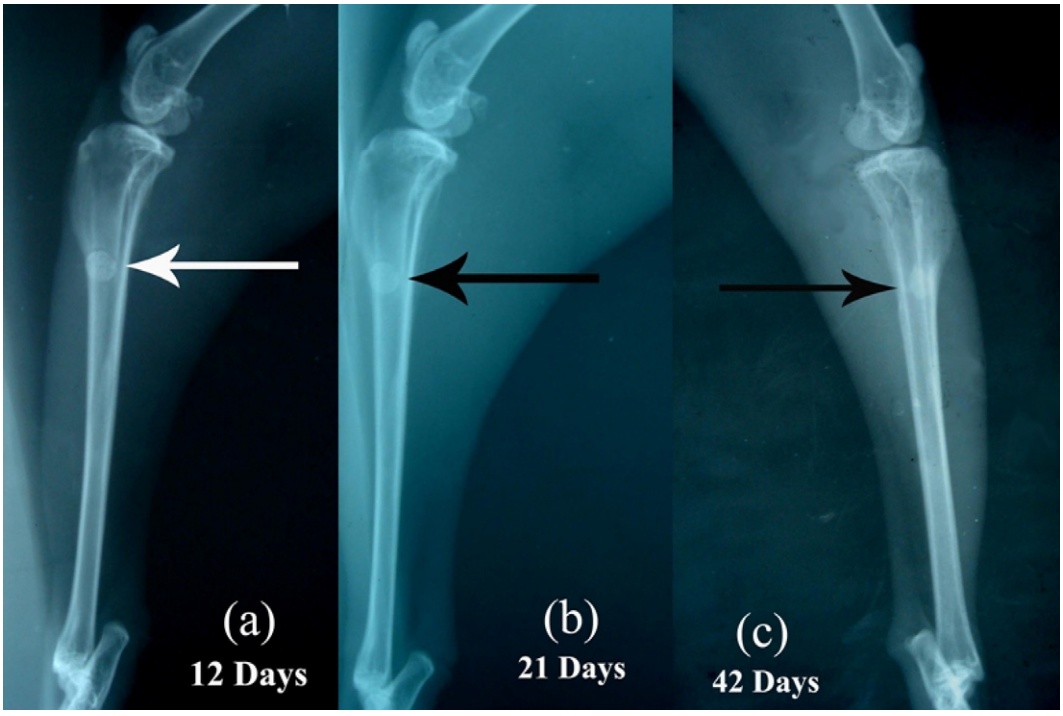

Fig. 14. Radiograph of the Group III animal.

drug release followed by a selection of desirable formulation that was further subjected to a six week animal trial. The pore percentage level has been considered earlier [12,31] only between 10 and 40%. Increasing the pore percentage further to 50 or 60 could provide results for better understanding and logical designing of porous TCP systems that could synergistically deliver drug and enhance bone formation. In the present study we have tried to address the above concerns by varying the pore conditions and confirmed the elution rate (*in vitro* in contact with PBS and SBF) before going into the detailed animal trials. Microstructure affected the adsorption and release behaviour both *in vitro* and *in vivo* [32]. For example, open porosity is most important because it is related to properties such as permeability and surface area. A bimodal distribution of pores are thought to be ideal for TCP to be used for sustained release of drug to the bone which not only includes large pores (more than 50 μm) to allow bone ingrowth into the pores but also small pores to facilitate the slow release of drug [33]. Most of the previous reports showed either the effect of low percentage of pores with presence of macropores that eluted drug very fast [34] or porous compacted granules which not only eluted drug in non-uniform rate but also degradation of calcium phosphate was another concern [20,35]. Increase in naphthalene content in the formulation resulted in lower porosity and hence higher bulk density of 60P. There was bimodal distribution of micropores in 50P samples and there

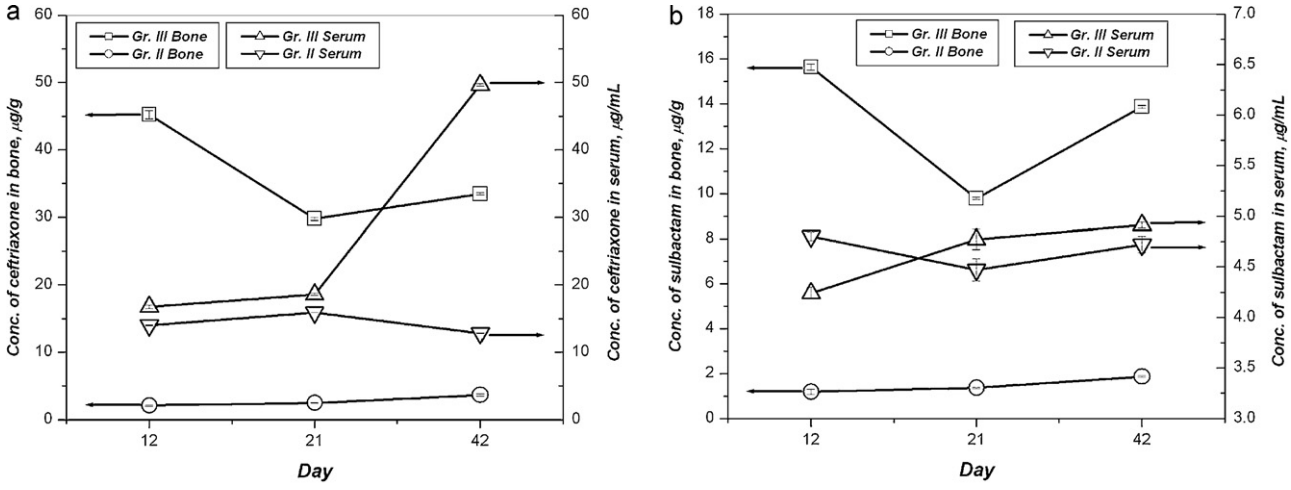

Fig. 15. *In vivo* concentration of (a) CFT and (b) SUL in different groups over different days interval. [Group II, parenteral injection of antibiotic; Group III, CFS-β-TCP implanted group].

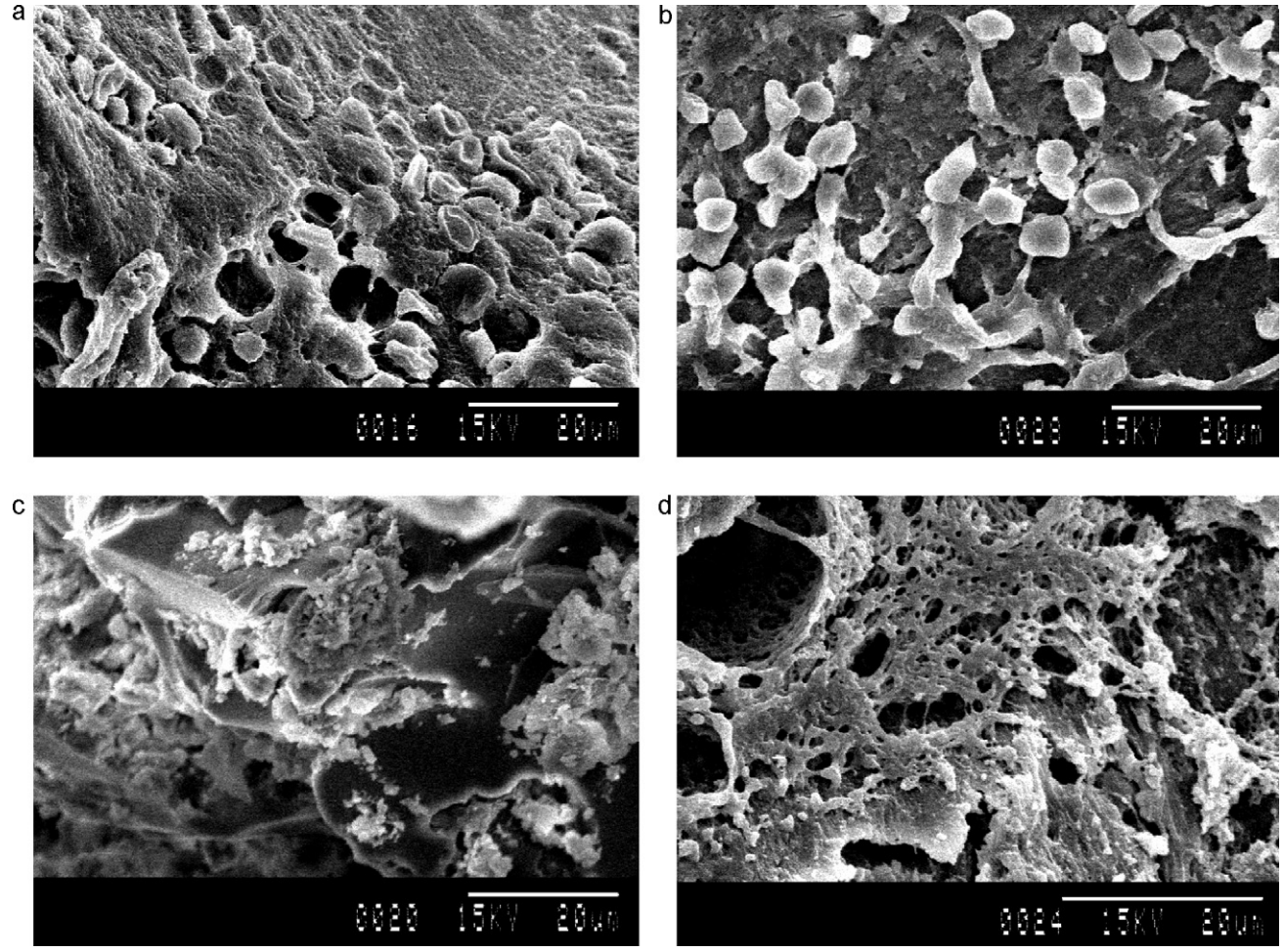

Fig. 16. Microstructures of bone defect sites for all the group of animals. (a) and (b) status of bone after 42 days when no treatment was provided (Group I) after development of osteomyelitis (i.e. control) and the site when parenterally treated (Group II) by CFS Group; (c) and (d) status of bone after 21 and 42 days when implanted with drug loaded porous TCP implants (Group III).

were more numbers of micropores in 50P than 60P samples. Due to the higher percentage of porosity and open pore surfaces in 50P, the adsorption efficiency of the drug increased. The presence of lesser amount of micropores in 50P samples also favoured high drug impregnation efficiency. This was also an indirect evidence of the better interconnectivity of pores in these samples. Pore interconnectivity is another important factor [36,37] often overlooked before scaffold design. Interconnected pores influence more critically than pore size alone.

Another parameter which also influences the drug attachment behaviour as well as degree of adhesion to the pore surface is the surface charge. Surface charge of TCP in aqueous media plays a significant role for drug attachment to the ceramic. This parameter in terms of zeta potential was particularly used for assessment of deflocculation characteristics while fabricating the porous HAp scaffold [38]. In our study, TCP surface in aqueous media at the physiological pH (7.4), had a moderately high negative zeta potential (ca. 27.2 mV) which was another factor responsible for better drug adhesion characteristics as evidenced from the values of adsorption efficiency as well as microstructure observed of CFS impregnated scaffolds. Recently negative surface charges of HAp have been reported to influence apatite nucleation, rapid cell attachment and faster tissue ingrowth [39,40], but there is no report to the best of our knowledge about the influence of this parameter of TCP for the same. With the high negative surface charges of the TCP scaffolds fabricated in this study in addition to drug attachment, accelerated mineral deposition, rapid cell attachment and faster tissue ingrowth could be expected.

CFS had many carboxylic groups which could form hydrogen bonds with the TCP surface and consequently drug molecules getting retained on the pore surface [41]. During drug loading, cations of both materials (i.e. ceramic and drug) inter-diffused and consequently EDAX showed small humps of the peaks corresponding to CFS in the microstructure of TCP and vice versa. There was no as such interface between these two materials (i.e. ceramic and drug) and the EDAX at the interface, showed mixture of above elements. One of the reasons for absence of interfacial gap between the drug and pore surface was due to electrostatic attraction between the functional groups of CFS and Ca^{2+} and PO_4^{3-} came from both β-TCP and α-calcium pyrophosphate. Further high adhesion

strength and subsequent cracks on the drug surface was due to higher surface potential on TCP surface, which contributed such phenomenon. From the drug point of view factors such as size [42], solubility [43] and binding capacity [44] to the biomaterial play a crucial role in the release of drugs. To elaborate, it should be quiet obvious for smaller molecules to easily pass through the pores and reach out faster when compared to bulkier molecules. So, the first step is to design the ceramic with high porosity and tailored pore number, size, shape, distribution and connectivity. The design again depends on the drug to be confined and subsequently released on the chemical nature of the wall, to achieve a greater control of the chemical interaction between the TCP and drug. Hence, the drug molecule included into the bioceramic matrix has to be considered. In general, the size of drug molecules fall within the nanometer scale and consequently, every porous material showing pore sizes higher than a few nanometers is expected to host these drug molecules. In addition, higher the solubility of drug, faster and greater would be its release. While comparing the drugs co-loaded in our study, sulbactam is a much smaller molecule than ceftriaxone with a molecular mass of 255.22 and 661.6 respectively. Sulbactam is readily soluble and ceftriaxone is freely soluble in water. In accordance with the generalizations it should be quite natural to expect a faster release of SUL and the same observed in SBF.

More elaborate release profiles were observed for 50P samples up to the total observation period. This was due to the prevalence of comparatively higher amount and bimodal distribution of micropores in these samples. 60P samples had both lesser numbers and sizes of micro- and macropores, which caused much slower diffusion of the attached drug *in vitro* in both PBS and SBF. According to Vallet-Regí et al., for drugs to be placed into pores, a material with homogeneous ordered pore distribution should be specially designed [41]. In such material, the drug adsorption and subsequent delivery will be more regular and reproducible than that coming from a disordered pore distribution. In the present study, we observed that more numbers of interconnected pores played a vital role more than the homogeneity of the pores. Homogeneity is more important for mesoporous solids than its interconnectivity for both binding and release of the drug *in vitro*. However, the binding capacity of the drug to the biomaterial is an important factor to retard the drug release. The –COOH groups present in the drug molecule are primarily responsible for binding with ceramic biomaterials and the intensity of binding increases with the number of available carboxyl groups [45]. Both the studied drugs have just one carboxyl group available. Hence, slower release of drug CFT could be due to (1) some other functional groups present in the CFT, which could have interacted to the TCP surface than that of SUL and (2) higher molecular weight and longer molecular chain than SUL.

SBF is an acellular fluid having inorganic ion concentrations similar (more than the composition of PBS) to those of human extra cellular fluid, mainly used to reproduce formation of apatite on bioactive materials *in vitro*. Since SBF composition is almost similar to our body physiological fluids in terms of its composition of ions, we expected release profiles of drugs obtained from SBF-soaked samples to be a more accurate prediction of the *in vivo* situation. This supersaturated solutions in contact with bioactive materials forms a layer of HAp thus covering the substrate with due course of time depending on the conditions of test, bioactive material subjected and composition of SBF selected. In the present investigation, faster but continuous release of the drugs were observed in SBF than with PBS, most probably due to non-formation of such layer which subsequently could have retarded the diffusion of drug molecule. Another reason could be presence of the phosphates contained in PBS decreases the hydrolysis of phosphate functional groups present in the sintered scaffold [46]. The more pronounced burst release of drugs in SBF than PBS may also be attributed to faster dissolution of β-TCP and α-$Ca_2P_2O_7$ in contact with SBF. Rai et al. [47] demonstrated that SBF-soaked composites of polycaprolactone–tricalcium phosphate had delayed release of biomolecules and absence of total release in the total study period owing to the polymer coating on TCP surface. Influences of other parameters however could be the same as explained earlier.

As to drug release mechanism, in general, the drug release pattern from porous calcium phosphates has been reported to be controlled by diffusion than matrix degradation [32,48]. In our case, 60P samples might have followed the same kinetics but in SBF, while 50P samples most probably degraded on comparison to 60P along with its drug elution in both PBS and SBF due to its high amount, size and prevalence of macropores over micro-pores. Finally, from the above observations we had selected the 50P samples for further animal trial owing to its 60–65% porosity with an average pore size ca. 55 μm, having higher interconnectivity (22–113 μm), moderately high CFS adsorption efficiency (ca. 79%) and finally with much slower, prolonged and homogeneous elution profile up to 42 days (higher than the MIC values) in contact with SBF.

From the SEM study of the bone–biomaterial interface of all groups it was found that Group III animals had far better bone ingrowth into the deep pores through the inter-pore connections after 21 days, which became matured at day 42. Our findings also corroborated the findings of Horowitz et al. [25] who used porous β-TCP implants alone, as replacement grafts, and found that it was completely resorbed and replaced by vital bone over six months time, where bovine derived grafts could not. Graft replacement ensures the regenerated bone will be able to remodel according to the stresses placed upon it in the future. In the present investigation however complete regeneration of bone was occurred very fast probably due to the sustained and maintenance of eluted drug from the porous β-TCP matrix which worked against recurrence of bacteria during the healing time. Intra-implant vascularization for group III animals' cortical site after 21 days had a favourable gradient for draining out of the drug CFS through capillary of the bone tissue, which was occurring even after 42 days. This finding also corroborated the findings of Castro et al. [49].

Histological observations provide more detailed knowledge about the cellular events during incorporation of different types of ceramic implants. Besides, best evidence of the efficiency of treatment of osteomyelitis could be observed in

histopathological and microbiological findings [50]. In Group II animals, chronicity of the disease observed after 42 days could be due to the fact that sufficient concentrations of antibiotic to destroy the organisms did not reach to the infected site due to presence of blood–bone barrier. For Group III animals however, the results observed after 42 days were very similar to the findings of Korkusuz et al. [51] who showed that osteomyelitic infection was subsided by 3 weeks and 6 weeks and inflammatory cells were replaced with bone forming cells upon treatment of osteomyelitis with antibiotic impregnated biodegradable implants. Similar findings were also observed by Sanchez et al. [52] in osteomyelitis model.

The treatment of osteomyelitis in orthopaedic surgery poses a great challenge due to improper and unsustained drug concentration at the site. Though the microbial organisms responsible for causing osteomyelitis are very much sensitive to different routinely used antibiotics *in vitro* but due to inherent characteristic of bony tissue, the success of treatment with such infections is very limited.

Radiographs taken for Group I animals had both osteophytic and lytic changes which were suggestive of osteomyelitis. Inflammation with hyperemia is the sequelae of bacterial contamination of bone, which ultimately leads to formation of abscess. The abscess continues to expand, with further production of purulent exudates [53]. The exudate enters the cortical bone and spreads across it via havarsian and volkman's canals and ultimately leading to necrosis of fragments of bone sequestrum and lyses [53,54].

Normal phenomenon of bone healing is formation of osteon in the phase of remodelling which aggregate in an acentric manner at any site of fracture area during the remodelling phase. In Group III, the desired level of antibiotic concentration at the site might have controlled the infections which in turn expedite the bone healing and remodelling as evidenced by newly grown periosteal bone. In similar finding, Korkusuz et al. [51] also reported radiographically mild periosteal elevation, architectural deformation, widening of bone shaft, new bone formation and soft tissue deformation after 6 weeks of implantation with Duocid and Sulperazone-loaded poly-hydroxybutyrate-co-hydroxyvalerate (PHBV) rods in rabbits. In another studies, radiological observations also showed beneficial effects and well toleration and gradual new bone formation with biodegradable and osteointegrable gentamicin bone implants [52].

Several biomaterials have been used as vehicles for the transport and sustained release of antibiotics. The pharmacokinetics of the composites *in vivo* showed that therapeutic concentration of antibiotic was maintained at the site of implantation which was adequate to provide antimicrobial activity. The reason for the efficacy of TCP in the treatment of osteomyelitis is probably the advantageous pharmacokinetics at the site of infection. The minimum inhibitory concentration (MIC) of ceftriaxone–sulbactum against *S. aureus* is 1 mg/L [15]. Concentrations exceeding the MIC were obtained around the implant in all bone tissues. The above results suggest that the composites in the present study fulfill this condition. On the whole, the maintenance of implant integrity and release of antibiotic at an adequate concentration indicates that this CFS loaded β-TCP implant was more effective compared with similar biodegradable, antibiotic releasing bone grafts. Normally, first order release is not desired and generally a constant release rate is aimed by the researchers. However, an early burst could actually be quite useful in the initial treatment of the microorganisms at the infection site, and the later, lower rate of release, could maintain the medium sterile. Macroporous beta tricalcium phosphate as antibiotic implant reported earlier maintained antibiotic concentrations in bone 5–10 times the MIC of *S. aureus* even at the end of 3 weeks [12]. Lambotte et al. reported though the macroporous beta tricalcium phosphate ceramic beads developed them studied by Norden's experimental osteomyelitis model with rabbit, maintained antibiotic concentrations in the bone for 10 days, the complete release of drug from the implant however happened within 3 days [31]. Nevertheless, full sterilisation of osteomyelitis was not achieved.Conclusions

In the present investigation, a novel and rational approach was made to combine drugs including an irreversible β-lactamase inhibitor with β-lactam antibiotic with a porous β-TCP scaffold, which can deliver the drug locally, and in a sustained fashion. Calcined (800 °C) β-TCP prepared by us was highly pure. Sintered TCP had ca. 14% of another calcium phosphate phase together with some amorphous content which probably had some control over subsequent drug attachment and bone regeneration. Porous β-TCP scaffolds exhibiting two kinds of pore percentage (50–55% and 60–65%) with similar distribution of pores sizes (average pore sizes were ca. 57.3 and 55.1 μm) have been studied in detail to cure osteomyelitis in animal model. It was established that 60–65% pore percentage with a distribution of bimodal micropores were found to be superior over the 50–55% porous samples both *in vitro* and *in vivo*. The criteria were matched with the 50P samples which had 60–65% porosity with an average pore size ca. 55.1 μm, having higher interconnectivity (22–113 μm), moderately high adsorption efficiency (ca. 79%) when loaded with CFS. CFS release from β-TCP implants were faster in SBF than PBS. Further, both the results of *in vitro* and *in vivo* drug elution after 42 days showed release higher than minimum inhibitory concentration of CFS against *S. aureus*. *In vivo* studies also proved the superiority of CFS loaded β-TCP implants than parenteral group based on eradication of infection and new bone formation.

Hence, for the first time we report the success of β-TCP in the form of porous scaffolds with designed porosity (in terms of micro- and macro-porosity, interconnectivity) to be an efficient and effective delivery system for antibiotics; which could locally and sustainably release the composite antibiotic (CFS) in reliable manner, both in terms of *in vitro* drug elution and *in vivo* animal trial leading to eradication of experimental chronic osteomyelitis. The physico-chemical nature of porous β-TCP surface and design of scaffolds modulated the confinement and delivery kinetics of the drug that is the consequences of results of both *in vitro* and *in vivo* experiments.

Acknowledgements

The authors wish to express their sincere thanks for the financial support by Department of Science and Technology,

India [T.1 (7)/TIFA/2006-CGCRI] and the Director, CSIR-CGCRI, India and Vice Chancellor, West Bengal University of Animal and Fishery Sciences, Kolkata, India for their generous and kind support to this work. All the personnel related to the characterization of the materials are sincerely acknowledged.

References

[1] C. Soundrapandian, S. Datta, B. Sa, Drug-eluting implants for osteomyelitis, Crit. Rev. Ther. Drug Carrier Syst. 24 (6) (2009) 493–545.
[2] L.O. Conterno, C.R. da Silva Filho, Antibiotics for treating chronic osteomyelitis in adults, Cochrane Database Syst. Rev. (Online) 3 (2009) CD004439.
[3] T.J. Houghton, K.S. Tanaka, T. Kang, E. Dietrich, Y. Lafontaine, D. Delorme, S.S. Ferreira, F. Viens, F.F. Arhin, I. Sarmiento, D. Lehoux, I. Fadhil, K. Laquerre, J. Liu, V. Ostiguy, H. Poirier, G. Moeck, T.R. Parr Jr., A.R. Far, Linking bisphosphonates to the free amino groups in fluoroquinolones: preparation of osteotropic prodrugs for the prevention of osteomyelitis, J. Med. Chem. 51 (21) (2008) 6955–6969.
[4] C. Soundrapandian, B. Sa, S. Datta, Organic–inorganic composites for bone drug delivery, AAPS PharmSciTech 10 (4) (2009) 1158–1171.
[5] S.K. Nandi, B. Kundu, S.K. Ghosh, T.K. Mandal, S. Datta, D.K. De, D. Basu, Cefuroxime-impregnated calcium phosphates as an implantable delivery system in experimental osteomyelitis, Ceram. Int. 35 (4) (2009) 1367–1376.
[6] S.K. Nandi, P. Mukherjee, S. Roy, B. Kundu, D.K. De, D. Basu, Local antibiotic delivery systems for the treatment of osteomyelitis – a review, Mater. Sci. Eng. C 29 (8) (2009) 2478–2485.
[7] R.Z. LeGeros, Calcium phosphate-based osteoinductive materials, Chem. Rev. 108 (11) (2008) 4742–4753.
[8] E.M. Bueno, J. Glowacki, Cell-free and cell-based approaches for bone regeneration, Nat. Rev. 5 (12) (2009) 685–697.
[9] T.A. Damron, Use of 3D beta-tricalcium phosphate (Vitoss) scaffolds in repairing bone defects, Nanomedicine (London, England) 2 (6) (2007) 763–775.
[10] M. Nakashima, A.H. Reddi, The application of bone morphogenetic proteins to dental tissue engineering, Nat. Biotechnol. 21 (9) (2003) 1025–1032.
[11] M. Mastrogiacomo, S. Scaglione, R. Martinetti, L. Dolcini, F. Beltrame, R. Cancedda, R. Quarto, Role of scaffold internal structure on in vivo bone formation in macroporous calcium phosphate bioceramics, Biomaterials 27 (17) (2006) 3230–3237.
[12] H. Thomazeau, F. Langlais, Antibiotic release by tricalcic phosphate bone implantation. In vitro and in vivo pharmacokinetics of different galenic forms, Chir. Mem. Acad. Chir. 121 (9–10) (1997) 663–666.
[13] K. Bush, S. Mobashery, How beta-lactamases have driven pharmaceutical drug discovery. From mechanistic knowledge to clinical circumvention, Adv. Exp. Med. Biol. 456 (1998) 71–98.
[14] K. Bush, The impact of beta-lactamases on the development of novel antimicrobial agents, Curr. Opin. Investig. Drugs 3 (9) (2002) 1284–1290.
[15] S.M. Shrivastava, S. Saurabh, D. Rai, V.K. Dwivedi, M. Chaudhary, In vitro microbial efficacy of sulbactomax: a novel fixed dose combination of ceftriaxone sulbactam and ceftriaxone alone, Curr. Drug Ther. 4 (1) (2009) 73–77.
[16] J.T. Mader, M.E. Shirtliff, S.C. Bergquist, J. Calhoun, Antimicrobial treatment of chronic osteomyelitis, Clin. Orthop. Relat. Res. 360 (1999) 47–65.
[17] B. Kundu, A. Lemos, C. Soundrapandian, P. Sen, S. Datta, J. Ferreira, D. Basu, Development of porous HAp and β-TCP scaffolds by starch consolidation with foaming method and drug–chitosan bilayered scaffold based drug delivery system, J. Mater. Sci. Mater. Med. 21 (11) (2010) 2955–2969.
[18] B. Kundu, M.K. Sinha, M.K. Mitra, D. Basu, Fabrication and characterization of porous hydroxyapatite ocular implant followed by an in vivo study in dogs, Bull. Mater. Sci. 27 (2) (2004) 133–140.
[19] B. Kundu, C. Soundrapandian, S. Nandi, P. Mukherjee, N. Dandapat, S. Roy, B. Datta, T. Mandal, D. Basu, R. Bhattacharya, Development of new localized drug delivery system based on ceftriaxone–sulbactam composite drug impregnated porous hydroxyapatite: a systematic approach for in vitro and in vivo animal trial, Pharm. Res. 27 (8) (2010) 1659–1676.
[20] M. Hasegawa, A. Sudo, V.S. Komlev, S.M. Barinov, A. Uchida, High release of antibiotic from a novel hydroxyapatite with bimodal pore size distribution, J. Biomed. Mater. Res. 70 (2) (2004) 332–339.
[21] T. Kokubo, H. Kushitani, S. Sakka, T. Kitsugi, T. Yamamuro, Solutions able to reproduce in vivo surface–structure changes in bioactive glass–ceramic A-W, J. Biomed. Mater. Res. 24 (6) (1990) 721–734.
[22] C.W. Norden, Experimental osteomyelitis. I. A description of the model, J. Infect. Dis. 122 (5) (1970) 410–418.
[23] R. Guinebretière, X-ray Diffraction by Polycrystalline Materials, ISTE, CA, USA, 2007, pp. 155–194.
[24] R.Z. LeGeros, Calcium phosphates in oral biology and medicine, in: H.M. Myers (Ed.), Monographs in Oral Science, vol. 15, Karger, Basel, 1991, pp. 4–45.
[25] R.A. Horowitz, Z. Mazor, C. Foitzik, H. Prasad, M. Rohrer, A. Palti, Beta-tricalcium phosphate as bone substitute material: properties and clinical applications, Int. J. Dent. Implants Biomater.: Titanium 1 (2) (2009) 2–11.
[26] D.G. Nelson, J.D. Featherstone, Preparation, analysis, and characterization of carbonated apatites, Calcified Tissue Int. 34 (Suppl. 2) (1982) S69–S81.
[27] T.R.N. Kutty, Assignments of some bands in the infrared spectrum of β-tricalcium phosphate, Ind. J. Chem. 8 (7) (1970) 655–657.
[28] S. Jinawath, D. Polchai, M. Yoshimura, Low-temperature, hydrothermal transformation of aragonite to hydroxyapatite, Mater. Sci. Eng. C 22 (1) (2002) 35–39.
[29] D. Basu, B. Mukherjee, Sintering of ceramics, in: S. Kumar (Ed.), Handbook of Ceramics, vol. 2, Kumar and Associates, Kolkata, 1997, pp. 168–181.
[30] M.P. Ginebra, T. Traykova, J.A. Planell, Calcium phosphate cements as bone drug delivery systems: a review, J. Control. Release 113 (2) (2006) 102–110.
[31] J.C. Lambotte, H. Thomazeau, G. Cathelineau, G. Lancien, J. Minet, F. Langlais, Tricalcium phosphate, an antibiotic carrier: a study focused on experimental osteomyelitis in rabbits, Chir. Mem. Acad. Chir. 123 (6) (1998) 572–579.
[32] D.J. Netz, P. Sepulveda, V.C. Pandolfelli, A.C. Spadaro, J.B. Alencastre, M.V. Bentley, J.M. Marchetti, Potential use of gelcasting hydroxyapatite porous ceramic as an implantable drug delivery system, Int. J. Pharm. 213 (1–2) (2001) 117–125.
[33] G.H. Walenkamp, L.L. Kleijn, M. de Leeuw, Osteomyelitis treated with gentamicin–PMMA beads: 100 patients followed for 1–12 years, Acta Orthop. Scand. 69 (5) (1998) 518–522.
[34] M. Itokazu, W. Yang, T. Aoki, A. Ohara, N. Kato, Synthesis of antibiotic-loaded interporous hydroxyapatite blocks by vacuum method and in vitro drug release testing, Biomaterials 19 (7–9) (1998) 817–819.
[35] H.H. Pham, P. Luo, F. Genin, A.K. Dash, Synthesis and characterization of hydroxyapatite–ciprofloxacin delivery systems by precipitation and spray drying technique, AAPS PharmSciTech 3 (1) (2002) E1.
[36] P.S. Eggli, W. Muller, R.K. Schenk, Porous hydroxyapatite and tricalcium phosphate cylinders with two different pore size ranges implanted in the cancellous bone of rabbits. A comparative histomorphometric and histologic study of bony ingrowth and implant substitution, Clin. Orthop. 232 (1988) 127–138.
[37] J.H. Kuhne, R. Bartl, B. Frisch, C. Hammer, V. Jansson, M. Zimmer, Bone formation in coralline hydroxyapatite. Effects of pore size studied in rabbits, Acta Orthop. Scand. 65 (3) (1994) 246–252.
[38] L.M. Rodriguez-Lorenzo, M. Vallet-Regi, J.M. Ferreira, Colloidal processing of hydroxyapatite, Biomaterials 22 (13) (2001) 1847–1852.
[39] S. Bodhak, S. Bose, A. Bandyopadhyay, Role of surface charge and wettability on early stage mineralization and bone cell-materials interactions of polarized hydroxyapatite, Acta Biomater. 5 (6) (2009) 2178–2188.
[40] S. Bodhak, S. Bose, A. Bandyopadhyay, Electrically polarized HAp-coated Ti: in vitro bone cell–material interactions, Acta Biomater. 6 (2) (2010) 641–651.

[41] M. Vallet-Regi, F. Balas, M. Colilla, M. Manzano, Drug confinement and delivery in ceramic implants, Drug Metab. Lett. 1 (1) (2007) 37–40.
[42] M. Vallet-Regí, L. Ruiz-González, I. Izquierdo-Barba, J.M. González-Calbet, Revisiting silica based ordered mesoporous materials: medical applications, J. Mater. Chem. 16 (1) (2006) 26–31.
[43] A. Lebugle, A. Rodrigues, P. Bonnevialle, J.J. Voigt, P. Canal, F. Rodriguez, Study of implantable calcium phosphate systems for the slow release of methotrexate, Biomaterials 23 (16) (2002) 3517–3522.
[44] A.E. Burgos, J.C. Belchior, R.D. Sinisterra, Controlled release of rhodium (II) carboxylates and their association complexes with cyclodextrins from hydroxyapatite matrix, Biomaterials 23 (12) (2002) 2519–2526.
[45] M. Stigter, J. Bezemer, K. de Groot, P. Layrolle, Incorporation of different antibiotics into carbonated hydroxyapatite coatings on titanium implants, release and antibiotic efficacy, J. Control. Release 99 (1) (2004) 127–137.
[46] R. Cini, D. Chindamo, M. Catenaccio, S. Lorenzini, E. Selvi, F. Nerucci, M.P. Picchi, G. Berti, R. Marcolongo, Dissolution of calcium pyrophosphate crystals by polyphosphates: an in vitro and ex vivo study, Ann. Rheum. Dis. 60 (10) (2001) 962–967.
[47] B. Rai, S.H. Teoh, K.H. Ho, An in vitro evaluation of PCL–TCP composites as delivery systems for platelet-rich plasma, J. Control. Release 107 (2) (2005) 330–342.
[48] T. Higuchi, Mechanism of sustained-action medication. Theoretical analysis of rate of release of solid drugs dispersed in solid matrices, J. Pharm. Sci. 52 (1963) 1145–1149.
[49] C. Castro, E. Sanchez, A. Delgado, I. Soriano, P. Nunez, M. Baro, A. Perera, C. Evora, Ciprofloxacin implants for bone infection. In vitro–in vivo characterization, J. Control. Release 93 (3) (2003) 341–354.
[50] U. Joosten, A. Joist, T. Frebel, B. Brandt, S. Diederichs, C. von Eiff, Evaluation of an in situ setting injectable calcium phosphate as a new carrier material for gentamicin in the treatment of chronic osteomyelitis: studies in vitro and in vivo, Biomaterials 25 (18) (2004) 4287–4295.
[51] F. Korkusuz, P. Korkusuz, F. Eksioglu, I. Gursel, V. Hasirci, In vivo response to biodegradable controlled antibiotic release systems, J. Biomed. Mater. Res. 55 (2) (2001) 217–228.
[52] E. Sanchez, M. Baro, I. Soriano, A. Perera, C. Evora, In vivo–in vitro study of biodegradable and osteointegrable gentamicin bone implants, Eur. J. Pharm. Biopharm. 52 (2) (2001) 151–158.
[53] T.W. Fossum, D.A. Hulse, Osteomyelitis, Semin. Vet. Med. Surg. (Small Animal) 7 (1) (1992) 85–97.
[54] M. Hoque, Post-traumatic osteomyelitis: its incidence in fracture case and experimental studies in goats, Indian Veterinary Research Institute, Izatnagar, India, 1996.